

Heteroclinic orbits and transport in a perturbed integrable Suris map*

Héctor E. Lomelí

Department of Mathematics
 Instituto Tecnológico Autónomo de México
 Mexico, DF 01000
 lomeli@gauss.rhon.itam.mx

James D. Meiss[†]

Department of Applied Mathematics
 University of Colorado
 Boulder, CO 80309
 jdm@boulder.colorado.edu

October 1, 2018

Abstract

Explicit formulae are given for the saddle connection of an integrable family of standard maps studied by Y. Suris. When the map is perturbed this connection is destroyed, and we use a discrete version of Melnikov's method to give an explicit formula for the first order approximation of the area of the lobes of the resultant turnstile. These results are compared with computations of the lobe area.

AMS classification scheme numbers: 34C35,34C37,58F05,70H15,70K99

Keywords: Integrable Maps, Melnikov Method, Transport, Twist maps

1 Introduction

Standard maps are area-preserving diffeomorphisms of $\mathbb{T} \times \mathbb{R}$ given by

$$(\theta', r') = f(\theta, r) = (\theta + r + V'(\theta), r + V'(\theta)), \quad (1)$$

*A version of this paper was originally written in 1996, but never published. Subsequently, the methods of this paper have been used and extended, for example by Delshams and Ramírez-Ros [1].

[†]JDM was supported in part by NSF grant number DMS-9971760.

where the potential, V , is periodic, $V(\theta + 1) = V(\theta)$. In this paper we study the standard map f_δ given by (1) with the potential¹

$$V_\delta(\theta) = -\frac{2}{\pi} \int_0^\theta dt \tan^{-1} \left(\frac{\delta \sin(2\pi t)}{1 + \delta \cos(2\pi t)} \right). \quad (2)$$

Suris [2, 3] showed that f_δ is integrable with integral

$$I_\delta(\theta, r) = \cos \pi r + \delta \cos \pi(2\theta - r),$$

i.e., $I_\delta \circ f_\delta = I_\delta$. Contours of I_δ are shown in Fig. 1. The map is integrable for any δ ; however, we will consider the case $0 < \delta < 1$, as the topology of the saddle connections changes at $\delta = 1$. For $0 < \delta < 1$ the map f_δ has hyperbolic fixed points at $z_a = (-\frac{1}{2}, 0)$ and $z_b = (\frac{1}{2}, 0)$, that are connected by two saddle connections, forming the upper and lower separatrices of the fixed point resonance.

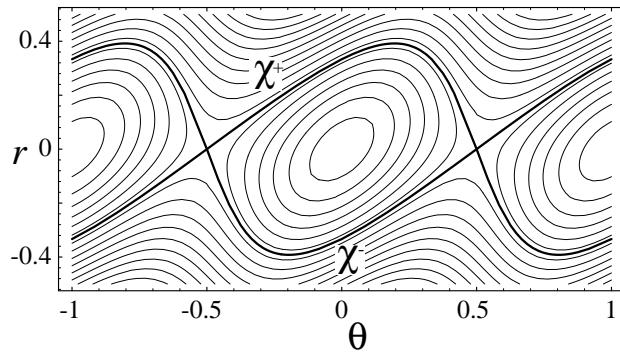


Figure 1: Some contours of I_δ , for $\delta = 1/3$.

Standard maps are examples of monotone twist maps (for a review, see [3]) defined by the geometrical *twist condition* that vertical lines tilt to the right upon iteration, $\frac{\partial \theta'}{\partial r} > 0$. Such maps have Lagrangian generating functions, $S(\theta, \theta')$, which generate the map implicitly through the equation $dS(\theta, \theta') = r'd\theta' - rd\theta$, or equivalently

$$r = -\partial_1 S(\theta, \theta'), \quad r' = \partial_2 S(\theta, \theta'), \quad (3)$$

where the subscripts indicate derivatives with respect the first and second arguments of S . The twist condition implies that $\partial_1 \partial_2 S < 0$. We assume that our twist map has *zero net flux*, which is equivalent to $S(\theta + 1, \theta' + 1) = S(\theta, \theta')$. For maps of the standard form, (1), the generating function is

$$S(\theta, \theta') = \frac{1}{2}(\theta' - \theta)^2 + V(\theta). \quad (4)$$

¹ The potential can also be written

$$V(\theta) = \frac{1}{\pi^2} \Re [\text{dilog}(1 + \delta) - \text{dilog}(1 + \delta e^{2\pi i \theta})].$$

where the dilogarithm is defined by $\text{dilog}(x) \equiv \int_1^x \frac{\log(z)}{1-z} dz$.

We will let S_δ denote the generating function for the Suris map f_δ .

Since the Suris map is integrable and has twist, Birkhoff's theorem [3] implies that the saddle connection between the equivalent points z_a and z_b is the graph of a function $r = \chi(\theta)$, for $\theta \in \bar{\mathcal{U}} = [-\frac{1}{2}, \frac{1}{2}]$. The dynamics (1) restricted to the saddle connection defines a circle diffeomorphism

$$\theta \mapsto h(\theta) = \theta + \chi(\theta) + V'(\theta).$$

Our goal is to show that, when the Suris map is perturbed, the stable and unstable manifolds of the continuation of the fixed points intersect transversely. We use a version of Melnikov's method [4] for twist maps [5, 6, 7, 8, 9, 10, 11]. The system is perturbed by adding to the original generating function any C^2 periodic function $P(\theta, \theta')$. We will assume for simplicity that P does not move the fixed points. Then for small enough ϵ , $S_\delta + \epsilon P$ is a twist generating function, and the corresponding map $f_{\delta, \epsilon}$ has hyperbolic fixed points at z_a and z_b . As was shown in [9], if the Melnikov potential, given by

$$L(\theta) = \sum_{t=-\infty}^{\infty} P(h^t(\theta), h^{t+1}(\theta)), \quad (5)$$

has a nondegenerate critical point in \mathcal{U} , then the manifolds $W^u(z_a, f_{\delta, \epsilon})$ and $W^s(z_b, f_{\delta, \epsilon})$ intersect transversely for ϵ small enough (the same conclusion is valid for $W^s(z_a, f_{\delta, \epsilon})$ and $W^u(z_b, f_{\delta, \epsilon})$). It is known that the series for L converges absolutely and uniformly to a C^2 function on compact subsets of \mathcal{U} . As an example below, we consider the case $P(\theta, \theta') = \cos^2 \pi\theta$.

Thus the potential L provides sufficient conditions for the transversal destruction of the saddle connection, just as in the classic applications of the Melnikov integral. In §2 we formulate a slightly stronger version of the previous result (Theorem 2).

The Melnikov potential also has a physical interpretation: the difference between values of L at neighboring critical points is the area of the turnstile lobe that they delineate. The area of the lobe gives a coordinate independent measure of the separation of the perturbed stable and unstable manifolds as well as the flux from one region to another (cf. [3]).

The sum for the order ϵ approximation for the lobe area is calculated explicitly in §3 and compared with numerical results in §4. We summarize our results, as

Theorem 1 (Main Theorem). *Let S_δ , given by (4) with potential V_δ (2), be the generating function for the integrable Suris map f_δ . Then*

$$S_{\delta, \epsilon} = S_\delta + \epsilon \cos^2 \pi\theta$$

generates a twist map $f_{\delta, \epsilon}$. For all $0 < \delta < 1$ and ϵ small enough there are two neighboring, primary heteroclinic orbits from $z_a = (-\frac{1}{2}, 0)$ to $z_b = (\frac{1}{2}, 0)$. The lobe defined by these two orbits has an area given by

$$A(\delta, \epsilon) = \epsilon\Gamma(\nu) + O(\epsilon^2) \quad (6)$$

where $\nu \equiv (1 - \sqrt{\delta})/(1 + \sqrt{\delta})$ and

$$\Gamma(\nu) \equiv 1 + 8 \sum_{k=1}^{\infty} \frac{(-1)^k k \nu^k}{1 + \nu^k} = \vartheta_4^4(0, \nu), \quad (7)$$

where $\vartheta_4(z, q)$ is the Jacobi theta function.

Note that the multipliers of the hyperbolic fixed point of f_δ are ν and $1/\nu$, so that ν is a natural parameter to use (see e.g., [11]).

The series $\Gamma(\nu)$ is rather intriguing. It is an analytic function of ν on the interval $\{0 < \nu < 1\}$, and approaches zero rapidly as ν increases. In fact, though (7) implies that $\Gamma(\nu)$ is strictly positive, it approaches zero exponentially fast:

$$\Gamma(\nu) \sim \left(\frac{4\pi}{\log(1/\nu)} \right)^2 \exp\left(\frac{-\pi^2}{\log(1/\nu)} \right)$$

as $\nu \rightarrow 1^-$, or equivalently $\delta \rightarrow 0^+$. However, note that (6) is only valid for fixed δ as $\epsilon \rightarrow 0$. If these parameters both approach zero, for example according to some relation $\delta = \delta(\epsilon)$, then the analysis becomes much more difficult. In particular when $O(\epsilon)$ term in (6) is exponentially small in δ , it could easily be dominated by terms that are formally higher order in ϵ .

2 Melnikov potential for twist maps

In this section we review the derivation of the Melnikov potential for twist maps [9]. We begin with a C^2 Lagrangian generating function $\tilde{S}(\theta, \theta')$ that satisfies the twist condition and has zero net flux. It gives a map of the annulus implicitly through (3). Alternatively, let the action W of a sequence $[\theta] = \{\theta^i, \theta^{i+1}, \dots, \theta^j\}$, be

$$W[\theta] = \sum_{t=i}^j \tilde{S}(\theta^t, \theta^{t+1}).$$

Then, an orbit of the map that begins at θ^i and ends at θ^j corresponds to a critical point of W under variation with respect to the interior points [3]. The corresponding momenta are then defined through (3) as $r^t = -\partial_1 \tilde{S}(\theta^t, \theta^{t+1})$. Thus, for example, a point (θ_a, r_a) is a fixed point of the map if and only if θ_a is a critical point of $\tilde{S}(\theta, \theta)$, and r_a is defined through (3).

The distance between the perturbed stable and unstable manifolds of any twist map with a saddle connection can be computed using the variational principle [12, 13]. We begin with a map \tilde{f} generated by \tilde{S} . Suppose that \tilde{f} has two hyperbolic fixed points $z_a = (\theta_a, r_a)$ and $z_b = (\theta_b, r_b)$, and there is a saddle connection defined by the graph of a function $\chi(\theta)$ on the interval $\mathcal{U} = (\theta_a, \theta_b)$ between these points. A diffeomorphism $h: \bar{\mathcal{U}} \rightarrow \bar{\mathcal{U}}$ is induced by the restriction of the map to the saddle connection:

$$\tilde{f}(\theta, \chi(\theta)) = (h(\theta), \chi(h(\theta))). \quad (8)$$

Let P be a C^2 function with zero net flux. Then the function

$$\tilde{S}_\epsilon(\theta, \theta') = \tilde{S}(\theta, \theta') + \epsilon \tilde{P}(\theta, \theta')$$

generates a twist map f_ϵ for small enough ϵ . Since hyperbolic points are nondegenerate critical points of the action [14], the perturbed map will have nearby hyperbolic fixed points for small enough ϵ . A simple case occurs when θ_a is a critical point of $\tilde{P}(\theta, \theta)$ as well as of $\tilde{S}(\theta, \theta)$ since it is then a critical point of $\tilde{S}_\epsilon(\theta, \theta)$ as well. Thus the fixed points of \tilde{S}_ϵ will have unchanged configurations, but their momenta will be modified according to (3).

The action gives useful formulae for the areas of regions for twist maps [15]. We will use one such relation to obtain the Melnikov potential: a relation between the graph χ and the action of orbits on the stable and unstable manifolds of a hyperbolic fixed point [16]. Let z^0 be a point on the unstable manifold of a fixed point z_a that is close enough to z_a so that the segment of $W^u(z_a)$ containing z^0 is given by a graph $(\theta, \chi(\theta))$. Let $(\theta^t, \chi(\theta^t)), t \leq 0$, be the preorbit of this z^0 . Defining the backward action difference as

$$\Delta W^B(\theta^0) = \sum_{t=-\infty}^{-1} \left[\tilde{S}(\theta^t, \theta^{t+1}) - \tilde{S}(\theta_a, \theta_a) \right],$$

then the unstable manifold is defined by the graph of the function

$$\chi^u(\theta) = \frac{\partial}{\partial \theta} \Delta W^B.$$

A corresponding formula for the forward action of an orbit on the stable manifold yields a formula for the graph of an initial segment of the stable manifold, χ^s , of z_b :

$$\begin{aligned} \Delta W^F(\theta^0) &= - \sum_{t=0}^{\infty} \left[\tilde{S}(\theta^t, \theta^{t+1}) - \tilde{S}(\theta_b, \theta_b) \right], \\ \chi^s(\theta) &= \frac{\partial}{\partial \theta} \Delta W^F. \end{aligned} \quad (9)$$

The difference between these two actions leads to the Melnikov-like formula for the transversal intersection of these manifolds. To summarize:

Theorem 2. *Let \tilde{S} be the generating function for a twist map \tilde{f} that has two hyperbolic fixed points z_a and z_b with a saddle connection given by $r = \chi(\theta)$ for $\theta \in \mathcal{U} = (\theta_a, \theta_b)$. Let \tilde{f} induce a diffeomorphism $h(\theta)$ on the connection. Let $\tilde{S}_\epsilon = \tilde{S} + \epsilon \tilde{P}$ generate the twist map \tilde{f}_ϵ , such that the perturbation \tilde{P} has the following properties*

- a) $\tilde{P}(\theta_a, \theta_a) = \tilde{P}(\theta_b, \theta_b) = 0$
- b) $\frac{d}{d\theta} \Big|_{\theta=\theta_a} \tilde{P}(\theta, \theta) = \frac{d}{d\theta} \Big|_{\theta=\theta_b} \tilde{P}(\theta, \theta) = 0$

Then for $\epsilon > 0$ small enough:

- i) the perturbed map has two hyperbolic fixed points near z_a and z_b ;

ii) *the Melnikov potential*

$$L(\theta) = \sum_{t=-\infty}^{\infty} \tilde{P}(h^t(\theta), h^{t+1}(\theta)) \quad (10)$$

converges absolutely and uniformly to a C^2 function on \mathcal{U} ; and

iii) *if L has a nondegenerate critical point on \mathcal{U} , then the unstable and stable manifolds of the two fixed points intersect transversely.*

We can relate the Melnikov potential to the area of a lobe in the stable and unstable manifolds using the action formula of [17]. Suppose p and q are two neighboring heteroclinic orbits, for example as shown in Fig. 2. Then the area lobe is determined by the difference in action between the orbits of p and of q [17]

$$A = \sum_{t=-\infty}^{\infty} \tilde{S}(\theta_q^t, \theta_q^{t+1}) - \tilde{S}(\theta_p^t, \theta_p^{t+1}) . \quad (11)$$

The area A is the signed area below the segment of W^s between q and p and above that of W^u .

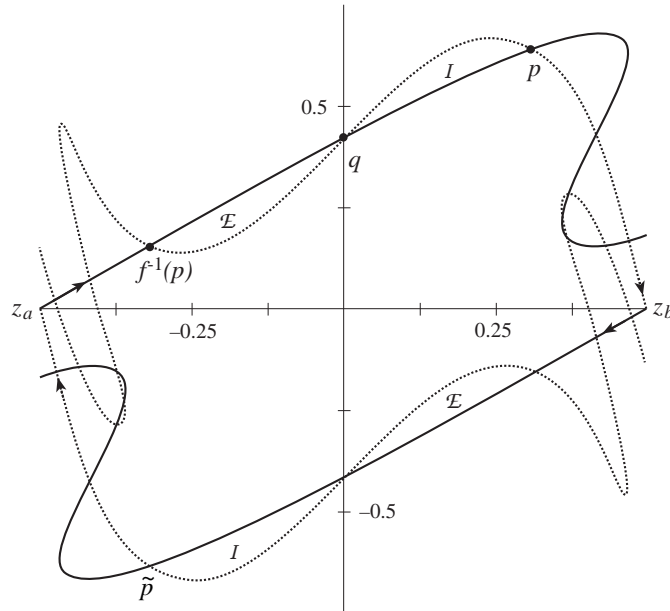


Figure 2: Resonance for the perturbed Suris map with $\delta = 0.5$ and $\epsilon = 0.05$. A pair of principal homoclinic points are labeled p and q , and the exit and incoming sets are labeled \mathcal{E} and \mathcal{I} .

Since the action is stationary on an orbit and since the actions of p and q are equal when there is a saddle connection, it is easy to see that the area of the lobe is determined, to lowest order, by the difference between two critical values of the Melnikov potential L (cf. [12, 13]). To summarize:

Theorem 3. *Let \tilde{S}_ϵ , \tilde{f}_ϵ , \mathcal{U} , h and L be defined as in Theorem 2. Assume that θ_p and θ_q are two points in \mathcal{U} such that*

- a) $L'(\theta_q) = L'(\theta_p) = 0$,
- b) $L''(\theta_p) > 0, L''(\theta_q) < 0,$
- c) $L'(\theta) \neq 0$ for $\theta_q < \theta < \theta_p.$

Then the heteroclinic points p and q continue to heteroclinic points of f_ϵ , and the stable and unstable manifolds of f_ϵ enclose a lobe with area

$$A(\epsilon) = \epsilon(L(\theta_q) - L(\theta_p)) + O(\epsilon^2) .$$

3 The Suris Map

We will use the results of the previous section with $\tilde{f} = f_\delta, \tilde{S} = S_\delta, \tilde{S}_\epsilon = S_{\delta,\epsilon}, \tilde{f}_\epsilon = f_{\delta,\epsilon}$ and the particular perturbation $\tilde{P}(\theta, \theta') = \cos^2 \pi\theta$. We give formulas for the lobe area of the perturbed Suris map. To find the saddle connection, we must find the diffeomorphism h induced by the dynamics of the Suris map f_δ on the connection (8). We will consider h defined only on the set $\mathcal{U} = \{-\frac{1}{2} < \theta < \frac{1}{2}\}$.

We first give some properties of h .

Lemma 4. *Let h be the diffeomorphism of $\bar{\mathcal{U}}$ given by*

$$h_\nu(\theta) = \frac{2}{\pi} \arctan \left(\frac{(\nu + 1) \tan(\frac{\pi}{2}\theta) + (\nu - 1)}{(\nu - 1) \tan(\frac{\pi}{2}\theta) + (\nu + 1)} \right) , \quad (12)$$

where $\nu = (1 - \sqrt{\delta})/(1 + \sqrt{\delta})$ and $0 < \delta < 1$. Then h_ν satisfies

- a) $h_\nu^t = h_{\nu^t}$, for all $t \in \mathbb{Z}$.
- b) $h_\nu(-\theta) = -h_{\nu^{-1}}(\theta)$.
- c) $-\frac{1}{2}$ is an stable fixed point and $\frac{1}{2}$ is a unstable fixed point of h_ν .
- d) $V'_\delta(\theta) = h_\nu(\theta) - 2\theta + h_\nu^{-1}(\theta)$, for $\theta \in \bar{\mathcal{U}}$, for V_δ given by (2).

Proof. A direct computation proves a) b) and c). This stability properties are implied by $h'_\nu(-\frac{1}{2}) = \nu$ and $h'_\nu(\frac{1}{2}) = \frac{1}{\nu}$. Since $\nu \in (0, 1)$ this implies that the former is stable and the latter is unstable. For d), we will first show that when $\theta \in \bar{\mathcal{U}}$,

$$\theta - h_\nu^{\pm 1}(\theta) = \frac{2}{\pi} \arctan \left(\frac{\pm \sqrt{\delta} \cos \pi\theta}{1 \mp \sqrt{\delta} \sin \pi\theta} \right) , \quad (13)$$

To see this, notice on one hand that if $\theta \in \mathcal{U}$, then $h(\theta) \in \mathcal{U}$. Therefore $-1 < \theta - h_\nu(\theta) < 1$. On the other hand,

$$\tan \left(\frac{\pi}{2} [\theta - h_\nu(\theta)] \right) = \frac{\sqrt{\delta} \cos \pi\theta}{1 - \sqrt{\delta} \sin \pi\theta} . \quad (14)$$

This implies (13) for the upper signs. The substitution $\theta \mapsto -\theta$ in equation (14), gives the lower signs. It is easy to see that if $\theta \in \mathcal{U}$, then (14) is positive and therefore $0 < \theta - h_\nu(\theta) < 1$. We conclude that for all $\theta \in \mathcal{U}$, $-1 < 2\theta - h_{\nu^{-1}}(\theta) - h_\nu(\theta) < 1$. To finish the proof we take tangent of the second difference and use the sum formula for tangent to obtain

$$\begin{aligned} \tan\left(\frac{\pi}{2}[2\theta - h_{\nu^{-1}}(\theta) - h_\nu(\theta)]\right) &= \frac{2\delta \cos \pi\theta \sin \pi\theta}{1 - \delta \sin^2 \pi\theta + \delta \cos^2 \pi\theta} \\ &= \frac{\delta \sin(2\pi\theta)}{1 + \delta \cos(2\pi\theta)}. \end{aligned}$$

Since this last expression is $-\tan(\frac{\pi}{2}V'_\delta(\theta))$, this completes the proof. \square

With the help of lemma 4, we can give a description of the intersection of the saddle connection between $(-\frac{1}{2}, 0)$ and $(\frac{1}{2}, 0)$. This connection is given by the functions χ^\pm , and is shown as the heavy curves in Fig. 1.

Lemma 5. *Let f_δ be the twist map generated by S_δ . Then $(-\frac{1}{2}, 0)$ and $(\frac{1}{2}, 0)$ are hyperbolic fixed points for f_δ and there are two saddle connections between them given by the graphs $r = \chi^+(\theta) = \theta - h_\nu(\theta)$, and $r = \chi^-(\theta) = \theta - h_{\nu^{-1}}(\theta)$.*

Proof. Using Lemma 4, the map can be written in the form

$$f_\delta(\theta, r) = (r + h_\nu(\theta) - \theta + h_{\nu^{-1}}(\theta), r + h_\nu(\theta) - 2\theta + h_{\nu^{-1}}(\theta)).$$

Therefore, if $r = \chi^-(\theta) = \theta - h_{\nu^{-1}}(\theta)$ then

$$f_\delta(\theta, \chi^-(\theta)) = (h_\nu(\theta), h_\nu(\theta) - \theta) = (h_\nu(\theta), \chi^-(h_\nu(\theta))).$$

Now since $\theta = -\frac{1}{2}$ is a stable fixed point for h_ν , this graph gives the left going saddle connection. In the same way setting $r = \chi^+(\theta) = \theta - h_\nu(\theta)$ gives

$$f_\delta(\theta, \chi^+(\theta)) = (h_{\nu^{-1}}(\theta), h_{\nu^{-1}}(\theta) - \theta) = (h_{\nu^{-1}}(\theta), \chi^+(h_{\nu^{-1}}(\theta))).$$

Since the map conjugates to $h_{\nu^{-1}}$ on this graph, this is clearly the right going saddle connection. \square

3.1 Proof of the Main Theorem

We now can sketch the proof of the main theorem. The analysis of the infinite series for the Melnikov potential relies on some summation formulae for elliptic integrals.

Proof. Let $P(\theta, \theta') = \cos^2 \pi\theta$. It is clear that P satisfies the conditions of Theorem 2. Let L be the Melnikov potential, (5). According to Theorem 2 a sufficient condition for transversal intersection of the perturbed manifolds is that L has a nondegenerate critical point on the interval $\mathcal{U} = \{-\frac{1}{2} < \theta < \frac{1}{2}\}$. The graph of $L(\theta)$ over \mathcal{U} is shown in Fig. 3.

To proceed, we define $\bar{L}(z) = L(\frac{2}{\pi} \arctan(z))$. A little algebra gives $\bar{L}(z) = \sum_{t=-\infty}^{\infty} \alpha_t(z)$ where

$$\alpha_t(z) = \frac{4\nu^{2t}(1-z^2)^2}{((1-z)^2 + \nu^{2t}(1+z)^2)^2}.$$

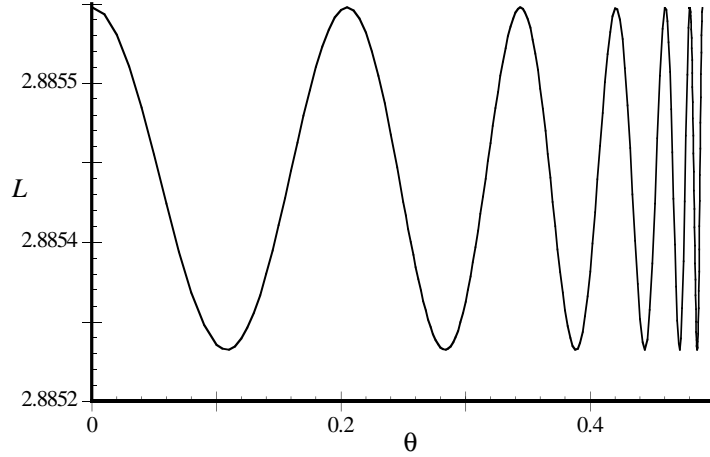


Figure 3: Melnikov potential, L for $\delta = 1/2$.

Since $z = \tan(\frac{\pi}{2}\theta)$ is monotone increasing, we need only show that there is a nondegenerate critical point of \bar{L} . We are going to show that $z_q = 0$ is a local maximum of \bar{L} and $z_p = (1 - \sqrt{\nu})/(1 + \sqrt{\nu})$ is a local minimum.

First, we write \bar{L} as

$$\bar{L}(z) = \alpha_0(z) + \sum_{t=1}^{\infty} \{\alpha_t(z) + \alpha_{-t}(z)\} . \quad (15)$$

Now, since $\alpha_t(-z) = \alpha_{-t}(z)$, this implies that \bar{L} is even, and so $\bar{L}'(0) = 0$. Differentiation gives

$$\bar{L}''(0) = -8 + \sum_{t=1}^{\infty} \frac{128(1 - 4\nu^{2t} + \nu^{4t})\nu^{2t}}{(1 + \nu^{2t})^4} \equiv -8\Gamma_0(\nu^2) .$$

This expression defines a function Γ_0 , which can be rewritten by expanding the denominator and rearranging the sums as

$$\Gamma_0(q) = 1 + 16 \sum_{k=0}^{\infty} \frac{(-1)^k k^3 q^k}{1 - q^k} .$$

This sum can be obtained from Fourier expansions of Jacobi elliptic functions which are written in terms of the nome, $q(k) = \exp(-\pi \frac{K'}{K})$, where $K(k)$ is the complete elliptic integral, $K' = K(k')$ and $k'^2 = 1 - k^2$ [18]. Recall that q is a monotone increasing diffeomorphism of k on $(0, 1)$. A Fourier expansion for elliptic functions [18, formula 912.01] can be differentiated to show that

$$\Gamma_0(q) = \left(\frac{2}{\pi} k' K \right)^4 = \vartheta_4^8(0, q) ,$$

where $\vartheta_4(z, q)$ is a Jacobi theta function [18, formula 1051.01]. Therefore $\bar{L}''(0) < 0$, for all $0 < \nu < 1$. This shows that $\theta_q = 0$ is a nondegenerate local maximum of L for all $0 < \nu < 1$.

We now wish to show that z_p is the local minimum. Rewrite \bar{L} as

$$\bar{L}(z) = \sum_{t=0}^{\infty} \{\alpha_{t+1}(z) + \alpha_{-t}(z)\} . \quad (16)$$

Since $\alpha_{t+1}(z_p + \zeta) = \alpha_{-t}(z_p - \zeta)$, \bar{L} is even around z_p , and so $\bar{L}'(z_p) = 0$. After some algebra, the second derivative is

$$\bar{L}''(z_p) = \sum_{t=0}^{\infty} \frac{(1 - 4\nu^{1+2t} + \nu^{2+4t})\nu^{1+2t}}{(1 + \nu^{1+2t})^4} .$$

Notice that $\bar{L}''(z_p) = \Gamma_0(\nu^2) - \Gamma_0(\nu)$. Once again, using Fourier series for elliptic functions, we find

$$\Gamma_0(q^2) = k'^2 \left(\frac{2}{\pi} K \right)^4 ,$$

so that

$$\bar{L}''(z_p) = \left(\frac{2}{\pi} K \right)^4 (kk')^2 ,$$

and therefore $\bar{L}''(z_p) > 0$, for all $0 < \nu < 1$. This shows that θ_p is a nondegenerate local minimum of L , for all $0 < \nu < 1$.

Using Theorem 3, we conclude that a lobe of area

$$A(\delta, \epsilon) = \epsilon(L(\theta_q) - L(\theta_p)) + O(\epsilon^2)$$

is enclosed by the stable and unstable manifolds, where θ_p and θ_q are given above. Finally, we use (15,16) to obtain

$$\begin{aligned} L(\theta_q) = \bar{L}(0) &= 1 + 8 \sum_{t=1}^{\infty} \frac{\nu^{2t}}{(1 + \nu^{2t})^2} , \\ L(\theta_p) = \bar{L}(z_p) &= 8 \sum_{t=0}^{\infty} \frac{\nu^{2t+1}}{(1 + \nu^{2t+1})^2} . \end{aligned}$$

Subtracting these two, and expanding the series we obtain

$$L(\theta_q) - L(\theta_p) = 1 + 8 \sum_{k=1}^{\infty} \frac{(-1)^k k \nu^k}{1 + \nu^k} = \Gamma(\nu) ,$$

where $\Gamma(\nu)$ was defined in (7). Finally, this result can be explicitly written as

$$\Gamma(q) = \left(\frac{2}{\pi} K k' \right)^2 = \vartheta_4^4(0, q) , \quad (17)$$

upon differentiating the Fourier series [18, 908.51] once. We have therefore obtained (6). \square

The explicit formula for the first order approximation of the area is compared with numerical computations in Sec. 4.

3.2 Exponentially small behavior

In this subsection we investigate the asymptotics of the sum, (7), as $\delta \rightarrow 0$. Our result is summarized as:

Lemma 6. *Let $\Gamma(\nu)$ be defined by (7), then*

$$\Gamma(\nu) \sim \left(\frac{4\pi}{\log(1/\nu)} \right)^2 \exp\left(\frac{-\pi^2}{\log(1/\nu)} \right) \text{ as } \nu \rightarrow 1^- . \quad (18)$$

Proof. We use the expression (17) in terms of the elliptic integral K and the nome q . Recall that $q \rightarrow 1^-$ as $k \rightarrow 1^-$ and $k' \rightarrow 0^+$. The needed asymptotic forms are [18, formulae 112.01 and 112.04]

$$\begin{aligned} K(k) &\sim \log\left(\frac{4}{k'}\right), \\ k' &\sim 4 \exp\left(-\frac{\pi^2}{2\log(1/q)}\right), \end{aligned}$$

as $k \rightarrow 1^-$. Putting these into (17) gives the promised result. \square

We again note that (18) does not imply that the area itself is necessarily exponentially small: (6) is only valid for fixed δ as $\epsilon \rightarrow 0$. Nevertheless we will see in §4 that (18) agrees remarkably well with our numerical calculations of the lobe area.

3.3 Anti-Integrable Limit

It is much easier to obtain an expression for the lobe area for large large ϵ . Our main purpose is to have an expression that is valid in the regime of large ϵ where numerical calculations are difficult. This expression is easy to obtain using the ‘‘anti-integrable limit’’ [19]. For simplicity, in this section we assume that P depends only upon θ in this section. In this case the anti-integrable limit is obtained by scaling the action by ϵ^{-1} , to get

$$\hat{S} = S(\theta, \theta')/\epsilon = P(\theta) + \epsilon^{-1}S_\delta ,$$

and then setting $\epsilon^{-1} = 0$. The point is that when $\epsilon \gg 1 > \delta$ the points on the two heteroclinic orbits are all found in a neighborhood of the critical points of the potential $P = \cos^2(\pi\theta)$, i.e., at $\theta = m/2$. In the anti-integrable limit, an orbit consists solely of a sequence of configuration points sitting at these critical points. Thus the two heteroclinic orbits are given by the sequences

$$\{\theta_p^t\} = \left\{ \dots, -\frac{1}{2}, -\frac{1}{2}, \frac{1}{2}, \frac{1}{2}, \dots \right\} , \quad \{\theta_q^t\} = \left\{ \dots, -\frac{1}{2}, -\frac{1}{2}, 0, \frac{1}{2}, \frac{1}{2}, \dots \right\}$$

The action is stationary on an orbit, thus to first order in the small parameter ϵ^{-1} , the change in the orbit with ϵ can be ignored in the action difference to give

$$\frac{1}{\epsilon}A = \sum_{t=-\infty}^{\infty} \left(\hat{S}(\theta_q^t, \theta_q^{t+1}) - \hat{S}(\theta_p^t, \theta_p^{t+1}) \right) + O(\epsilon^{-2}) .$$

For the Suris map, this yields

$$A(\delta, \epsilon) = \epsilon - \frac{1}{4} - \frac{1}{\pi^2} [\text{dilog}(1 + \delta) - \text{dilog}(1 - \delta)] + O(\epsilon^{-1}) \quad (19)$$

We compare this result with the numerical calculations in §4.

4 Numerical comparison

In this section, we compare the theoretical results with numerical computations of the lobe area. The task is to find the actions of the two homoclinic points p and q . For this task we use the symmetry of the Suris map. The action difference between the orbits of q and p gives the lobe area, (11).

The Suris map is reversible: it is conjugate to its inverse by an involution $R: R^2 = I$ and $Rf_\delta R = f_\delta^{-1}$, where the reversor is

$$R: (\theta, r) \rightarrow (-\theta, r + V'(\theta)). \quad (20)$$

Fixed sets, $\text{Fix}(R) = \{(\theta, r) : \theta = 0\}$ and $\text{Fix}(f_\delta R) = \{(\theta, r) : r = 2\theta\}$ of the reversor are important because points $q \in W^u(z_a) \cap \text{Fix}(R)$ or $q \in W^u(z_a) \cap \text{Fix}(f_\delta R)$ are heteroclinic from z_a to z_b [20]. Thus to find a heteroclinic orbit it is sufficient to do a one dimensional search for points on the unstable manifold that intersect one of these fixed sets.

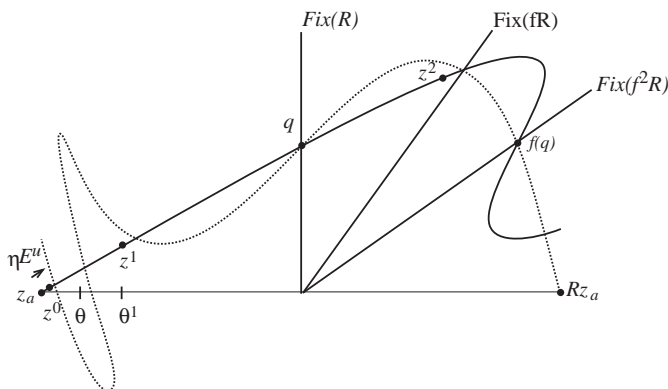


Figure 4: Finding some heteroclinic orbits using symmetry. Shown are the fixed sets $\text{Fix}(f^t R)$, for $t = 0, 1, 2$ and a rough example of initial guess z_0 , leading to $t_c = 1$.

To find these orbits numerically we move along $W^u(z_a)$ to the first points that intersect $\text{Fix}(R)$ and $\text{Fix}(fR)$, respectively. For example, to find $q \in \text{Fix}R$, let $z^0 = (\theta^0, r^0) = z_a + \eta E^u$ where E^u is the unstable eigenvector, and η is a small parameter to be chosen below. Let $t_c + 1$ be the first time for which the iterate of z^0 is beyond $\text{Fix}(R)$. Now choose a point $z(\theta)$ on the line from z^0 to $z^1 = f_\delta(z^0)$, parameterized by the initial angle θ . By construction we are guaranteed that the function $Z(\theta) = \pi_1 f_\delta^{t_c}(z(\theta))$ has a zero for $\theta \in [\theta^0, \theta^1]$. We use a root finding method (Brent's method) to determine this zero to some precision, say ρ . The choice of precision influences the original value for η , as well as the number of iterates until a crossing. Assuming W^u is smooth, the point z^0 will be

$O(\eta^2)$ away from W^u . After t_c iterates, however, this error will decrease by the factor λ^{-t_c} where λ is roughly the unstable multiplier of the fixed point. There is no sense in having this error smaller or larger than the precision of our root finder, so we set $\rho \sim \lambda^{-t_c} \eta^2$. On the other hand, since we start a distance η from the fixed point, and wish to go a distance $O(1)$ to find the first crossing of the symmetry line, we have $\eta \lambda^{t_c} = O(1)$. Thus, it is appropriate to set $\eta \sim \rho^{1/3}$. To find the second homoclinic point, $p \in \text{Fix}(f_\delta R)$, we repeat the above analysis, using crossing of $\text{Fix}(f_\delta R)$ to determine t_c , etc. The lobe area is given by the difference in action between these two orbits, from (11).

For our computations, using IEEE double precision arithmetic, we set $\rho = 10^{-19}$. These computations give apparently accurate results providing $A \gg 10^{-14}$. Subsequent to our obtaining these results, Delshams and Ramírez-Ros used extended precision arithmetic to obtain lobe areas as small as 10^{-4200} [1].

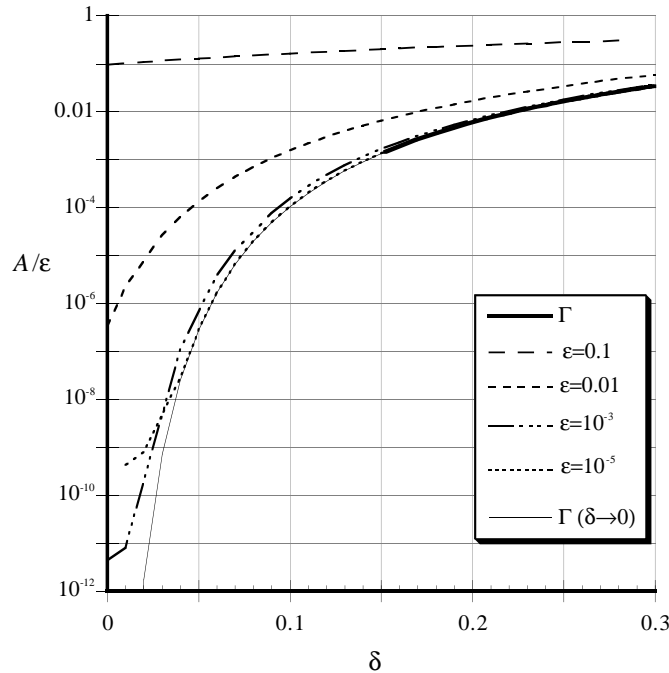


Figure 5: Log-Linear plot of A/ϵ as a function of δ for various values of ϵ compared with the theoretical expression (6) (thick line) and the small δ expression (18) (thin line)

In Fig. 5 we show a comparison of the result of (6) with the numerical results on a log scale. The analytical result agrees well with the numerical results when $\epsilon = 10^{-5}$. We show the same data on a linear scale in Fig. 6. We plot the sum (7) only for $\delta > 0.15$, since it is indistinguishable from asymptotic formula (18) for smaller values. Moreover, the asymptotic formula agrees with the $\epsilon = 10^{-5}$ computation within 1% up to $\delta = 0.8$. In Fig. 6, the anti-integrable results evaluated at $\epsilon = 1$ are also shown. We are unable to obtain numerical results for such a large ϵ , as the multiplier of the fixed points is too large.

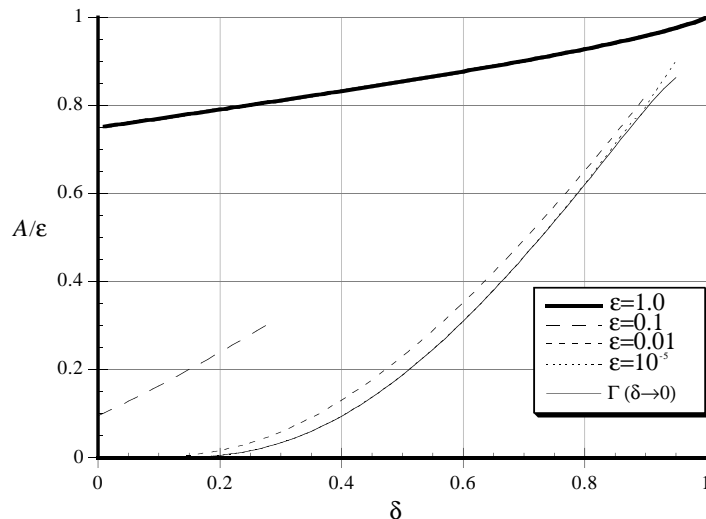


Figure 6: Linear plot of A/ϵ as a function of δ for various values of ϵ . The solid curve is the anti-integrable limit (19) for $\epsilon = 1$.

5 Conclusion

The perturbed Suris map studied here depends on two parameters, the Suris parameter δ and the perturbation strength ϵ . We obtained the lobe area for the fixed point resonance of this map for small ϵ to $O(\epsilon)$ and for large ϵ to $O(\epsilon^{-1})$. In the small epsilon case, the numerical computations indicate that the asymptotic formula (18) for $\delta \rightarrow 0$ is a good approximation even up to $\delta = 0.8$.

A similar Melnikov analysis is possible for other standard maps [7, 11]. In particular [9] showed that there exists a large class of standard maps with saddle connections. Interestingly these maps are not all integrable. The use of the Melnikov potential is not restricted to twist maps; in fact, it can be applied to any exact symplectic map [13].

The method can also be applied to any higher dimensional twist map that has a saddle connection of the type described in this paper (see [13, 10]). Integrable examples of such maps have been found in [21, 22, 23], and the Melnikov method has been applied to applied to the four dimensional McLachlan map [13]. Similar techniques are also applicable to volume preserving maps [24]. The study of perturbations of twist maps with saddle connections in higher dimensions is important because it could help in the development of a higher dimensional theory of transport.

References

- [1] A. Delshams and R. Ramírez-Ros. Singular separatrix splitting and the Melnikov method: an experimental study. *Experiment. Math.*, 8(1):29–48, 1999.
- [2] Yu. B. Suris. Integrable mappings of the standard type. *Func. Anal. and Appl.*, 23:74–76, 1989.

- [3] J.D. Meiss. Symplectic maps, variational principles, and transport. *Rev. Mod. Phys.*, 64(3):795–848, 1992.
- [4] V.K. Melnikov. On the stability of the center for time periodic perturbations. *Trans. Moscow Math. Soc.*, 12:1–57, 1963.
- [5] R.W. Easton. Computing the dependence on a parameter of a family of unstable manifolds: Generalized Melnikov formulas. *Non. Anal. Th. Meth. and Appl.*, 8:1–4, 1984.
- [6] M.L. Glasser, V.G. Papageorgiou, and T.C. Bountis. Melnikov’s function for two-dimensional mappings. *SIAM J. Appl. Math.*, 49:692–703, 1989.
- [7] A. Delshams and R. Ramírez-Ros. Poincaré-Melnikov-Arnold method for analytic planar maps. *Nonlinearity*, 9(1):1–26, 1996.
- [8] H. Lomelí. Perturbations of elliptic billiards. *Phys. D*, 99:59–80, 1996.
- [9] H. Lomelí. Saddle connection and heteroclinic orbits for standard maps. *Nonlinearity*, 9:649–668, 1996.
- [10] H. Lomelí. Applications of the Melnikov method to twist maps in higher dimensions using the variational approach. *Erg. Th. and Dyn. Sys.*, 17:445–462, 1997.
- [11] A. Delshams, R. Ramírez Ros, and T.M. Seara. Splitting of separatrices in Hamiltonian systems and symplectic maps. In C. Simo, editor, *Hamiltonian Systems with Three or More Degrees of Freedom*, volume 533 of *Series C: Mathematical and Physical Sciences*, pages 39–54. Kluwer Academic, 1999.
- [12] R.S. MacKay and J.D. Meiss. Relationship between quantum and classical thresholds for multiphoton ionization of excited atoms. *Phys. Rev. A*, 37(12):4702–4706, 1988.
- [13] A. Delshams and R. Ramírez-Ros. Melnikov potential for exact symplectic maps. *Comm. Math. Phys.*, 190(1):213–245, 1997.
- [14] R.S. MacKay and J.D. Meiss. Linear stability of periodic orbits in Lagrangian systems. *Phys. Lett. A*, 98:92–94, 1983. Relation between Residue and second variation of action.
- [15] R.S. MacKay, J.D. Meiss, and I.C. Percival. Resonances in area preserving maps. *Phys. D*, 27:1–20, 1987.
- [16] E. Tabacman. Variational computation of homoclinic orbits for twist maps. *Phys. D*, 85:548–562, 1995.
- [17] R.S. MacKay, J.D. Meiss, and I.C. Percival. Transport in Hamiltonian systems. *Phys. D*, 13:55–81, 1984.
- [18] P.F. Byrd and M.D. Friedman. *Handbook of Elliptic Integrals*. Springer-Verlag, 1971.

- [19] R.S. MacKay and J.D. Meiss. Cantori for symplectic maps near the anti-integrable limit. *Nonlinearity*, 5:149–160, 1992.
- [20] D. Sterling, H.R. Dullin, and J.D. Meiss. Homoclinic bifurcations for the Hénon map. *Physica D*, 134(2):153–184, 1999.
- [21] R.I. McLachlan. Integrable four-dimensional symplectic maps of standard type. *Phys. Lett. A*, 177(3):211–214, 1993.
- [22] J. Moser and A. Veselov. Discrete versions of some classical integrable systems and factorization of matrix polynomials. *Commun. Math. Phys.*, 139:217–243, 1991.
- [23] Yu. B. Suris. A discrete-time Garnier system. *Phys. Lett. A*, 189:281–289, 1994.
- [24] H. E. Lomelí and J.D. Meiss. Heteroclinic primary intersections and codimension one Melnikov method for volume preserving maps. *Chaos, in press*, 1999.